

RSC Advances



This is an *Accepted Manuscript*, which has been through the Royal Society of Chemistry peer review process and has been accepted for publication.

Accepted Manuscripts are published online shortly after acceptance, before technical editing, formatting and proof reading. Using this free service, authors can make their results available to the community, in citable form, before we publish the edited article. This *Accepted Manuscript* will be replaced by the edited, formatted and paginated article as soon as this is available.

You can find more information about *Accepted Manuscripts* in the [Information for Authors](#).

Please note that technical editing may introduce minor changes to the text and/or graphics, which may alter content. The journal's standard [Terms & Conditions](#) and the [Ethical guidelines](#) still apply. In no event shall the Royal Society of Chemistry be held responsible for any errors or omissions in this *Accepted Manuscript* or any consequences arising from the use of any information it contains.



Journal Name

ARTICLE

Enhanced electrochemical performance of NiO by addition of sulfonated graphene for supercapacitor

Lin Wang^{*a}, Hua Tian^a, Lin Zhang^a, Faming Gao^a, Jianmin Gu^a, Li Hou^a, Yang Jiang^a, Cunqi Wu^{*b}Received 00th January 20xx,
Accepted 00th January 20xx

DOI: 10.1039/x0xx00000x

www.rsc.org/

A facile approach for the fabrication of NiO/sulfonated graphene composites (NiO/SGNS) using ammonium carbamate as a precipitating agent was developed. For the enhanced specific surface and desirable surface chemical environment, NiO/sulfonated graphene composites exhibit excellent electrochemical performance. The results from cyclic voltammetry (CV) demonstrate that traditional electrical double-layer capacitive processes contribute to improve the storage energy capability of NiO/SGNS composites. Galvanostatic charge-discharge tests show that the specific capacitance of NiO/sulfonated graphene composites is increased to 530 F g⁻¹ at a current density of 1.0 A g⁻¹ in comparison with the specific capacitances of 382 F g⁻¹ for NiO/thermal reduced graphene composites (NiO/TRG) and 238 F g⁻¹ for pristine NiO. Moreover, electrochemical impedance spectroscopy (EIS) indicates the considerable effect of sulfonated graphene on building electron and ion transport channels for Faradic reaction processes of NiO/SGNS composites.

1. Introduction

To drop the environmental pollution arising from the industrial, urban and vehicular combustion of fossil fuels, the development of renewable and sustainable energy imposes new challenges to high power and energy storage devices.¹⁻³ Supercapacitor has attracted a deal of attention, which can bridge the gap between conventional capacitors and rechargeable batteries for electronic devices.⁴⁻⁸ The novel characteristic of electrode materials is a crucial issue in the competition of various energy storage devices. Among all the candidate materials, considerable efforts have been devoted to the research on NiO as a pseudocapacitive material, because of its high theoretical specific capacitance, low cost, and high chemical stability.⁹⁻¹²

However, the commercial application of NiO suffers from its low electrical conductivity and inferior electrolyte compatibility. To tackle these problems, carbon-based materials (carbon nanotubes, activated carbon, mesoporous carbons and so on) are very popular to be employed to improve electrochemical performance of this metal oxide.¹³⁻¹⁶ Mesoporous carbons, which were obtained from the carbonization for plant-derived lignin precursors, could embed highly dispersed NiO nanoparticles by liquid-crystalline phase-templating approach.¹⁷ Meanwhile, the high surface area, uniform pore sizes, various porous distributions and large pore volumes of NiO-containing mesoporous carbon materials ensured that they had the high specific capacitance and good cycle stability. The study on capacitive properties of the core-shell structure carbon aerogel microbeads-nanowhisker-like NiO composites shown that the improvement of electrochemical behaviors for these composite materials was

attributed to the combination of electrical double-layer capacitance of carbon aerogel microbeads and pseudo-capacitance based on the redox reaction of NiO.¹⁸

Moreover, graphene with a two-dimensional honeycomb lattice structure of graphite could also improve electrochemical performance of metal oxide due to its unique properties with ultra large surface area and extremely high electrical conductivity.¹⁹⁻²⁰ Hence, the application of NiO/graphene composites for supercapacitors has been energetically attempted. P.Q. Cao *et al.* successfully synthesized mesoporous NiO/RGO composites through a facile hydrothermal method.²¹ The as-prepared composites had a unique 3D network structure consisting of graphene sheets and anchored NiO particles, which could increase the contact between electrolytes and active materials, as well as shorten ion diffusion paths. Y.M. Chen *et al.* synthesized a hybrid material composed of high density graphene/NiO by microwave-assisted *in situ* method of NiO at the defects of graphene.²² The composite electrodes exhibited good cycle performance because of that the uniform dispersion of NiO nanoparticles on graphene sheets and the larger distance between neighboring graphene sheets provided enough spaces to buffer the volume change of NiO nanoparticles during charge-discharge redox reaction.

However, graphene lacks the hydrophilic character and tends to form irreversible agglomeration, limiting the formation of uniform graphene-based composites by conventional process methods. To overcome these drawbacks, sulfonated graphene with strong hydrophilic properties and the high specific surface has been introduced. Recently, many researches have demonstrated that the electrical conductivity and electrochemical performance of sulfonated graphene are superior compared to those of pristine graphene.²³

Importantly, sulfonated graphene is highly effective to strengthen the chemical adsorption of various ions on carbon nanosheets, which is conducive to assemble hierarchical graphene-based composites with enhanced electrochemical performance.²⁴⁻²⁶

In the previous work,²⁷ we fabricated NiO/sulfonated graphene composites via hydrothermal method. The porous structure of NiO/sulfonated graphene composites resulting from the adsorption of urea on sulfonated graphene via ionic bonding improves electrochemical properties rather than NiO/thermal reduced graphene composites. However, how to consolidate the effect of sulfonated graphene on electrochemical behaviors of NiO is still an interesting issue for supercapacitors. In this work, NiO/sulfonated graphene composites are assembled using ammonium carbamate as a precipitating agent. Moreover, the presence of absolute alcohol as a solvent in the fabrication process weakens hydrogen bonding between solvent molecules and sulfonated graphene, strengthening the positive effect of sulfonated graphene on microstructures and electrochemical properties of NiO.

2. Experimental section

2.1. Reagents.

Reagents were commercially obtained and used without further purification. Graphite oxide(GO) was synthesized from natural graphite powders by a modified Hummer's method.²⁸ Thermal reduced graphene(TRG) was obtained after graphite oxide being put into a muffle oven preheated to 800 °C for 60 s.²⁹

2.2 Synthesis of sulfonated graphene

Sulfonated graphene was synthesized from thermal reduced graphene following procedures described in the literature.³⁰ Of thermal reduced graphene, 80 mg was dispersed in 30 mL of deionized water by mild sonification. The above sample was sulfonated with 2.1 g of aryl diazonium salt of sulfanilic acid in an ice bath for 1 h. Subsequently, 100 mL of absolute alcohol was added, and then stirred for 1 h. The obtained sulfonated graphene was washed with 3 wt% HCl aqueous solution and deionized water, and then dried at 60 °C overnight.

2.3 Synthesis of NiO/sGNS composites

NiO/sGNS composites were synthesized through a two-step synthetic method. The typical route was as follows: 20 mg of sulfonated graphene and 230 mg of nickel nitrate hexahydrate were added into 50 mL of absolute alcohol. The mixture was treated with ultrasonic waves for 30 min, and then was stirred at 70 °C for 12 h. Then, 120 mg of ammonium carbamate was added into the above solution, and the mixture was stirred at 70 °C for additional 2 h. Afterward, the resulting product was filtered, washed with distilled water and absolute alcohol several times, and then dried at 60 °C for 12 h in a vacuum oven. Subsequently, NiO/sGNS composites were obtained through thermal treatment of the above product at 350 °C in

air for 3 h. For comparison, pristine NiO and NiO/TRG composites were prepared by the similar method.

2.4 Materials characterization

Powder X-ray diffraction(XRD) analysis was performed on Rigaku D/MAX-RC X-ray diffractometer in order to identify crystalline phases of materials. Morphologies of products as prepared were observed on a transmission electron microscopy(TEM, Hitachi, H-7700, 100 kV) and a field emission scanning electron microscopy (FESEM, Hitachi, S-4800, 15 kV). X-ray photoelectron spectroscopy(XPS) measurements were carried out on a Kratos Axis Ultra-dld spectrometer equipped with a monochromatic Al-K radiation($h\nu = 1486.6$ eV). The carbonaceous C 1s line(284.6 eV) was used as the reference to calibrate the binding energies(BEs). The nitrogen adsorption-desorption spectra of the samples were obtained by Brunauer-Emmett-Teller(BET) measurements using Quantachrome Autosorb-1C-VP at 77 K. The specific surface was calculated via BET method in the relative pressure range of 0.01-0.3, and the pore size distribution was calculated using adsorption branches of nitrogen adsorption-desorption isotherms by BJH method.

2.5 Electrochemical measurement

Cyclic voltammetry curves and galvanostatic charge-discharge tests of electrodes as prepared were investigated under a conventional three-electrode cell with 6 mol L⁻¹ KOH aqueous solution as electrolytes in the potential range of 0 to 0.5 V(vs. Hg/HgO) at room temperature. The working electrode was fabricated by mixing powders as prepared with 20 wt% acetylene black and 10 wt% polytetrafluorene ethylene(PTFE) binder. A small amount of distilled water was added to the mixture to produce a homogeneous paste. The mixture was pressed onto nickel foam current collectors (1.0 cm × 1.0 cm) to make electrodes. The mass of the active material in a single electrode was around 2 mg. A platinum foil and an Hg/HgO electrode served as the counter and reference electrode respectively. CV curves were conducted on a CHI 660E electrochemical workstation(Shanghai CH Instrument Company, China). Galvanostatic charge-discharge tests were investigated by a Neware battery testing workstation.

3. Results and discussion

The chemical compositions of all the samples obtained are characterized by XRD in Fig. 1. It is clearly found that the peaks appear at 37.1, 43.2 and 62.8° corresponding to (111), (200) and (220) crystal planes of cubic NiO (JCPDS 65-2901). Both the composites exhibit the similar profile to pristine NiO, due to disordered stacking of graphene in composites and quite uniform dispersion of metal oxide on the surface of two-dimensional carbon materials. Remarkably, the peak half-width is gradually increased in the sequence of pristine NiO, NiO/TRG composites and NiO/sGNS composites, suggesting that the growth of NiO grains is obviously inhibited due to that hydrophilic configurations of sGNS enhance the adsorption of

nickel cations on carbon nanosheets in absolute alcohol. The average sizes of NiO crystals calculated by the Scherrer equation ($D=0.89/\lambda \cos \theta$) based on the (200) reflection are 8.7, 5.8 and 5.3 nm for NiO, NiO/TRG composites and NiO/sGNS composites.

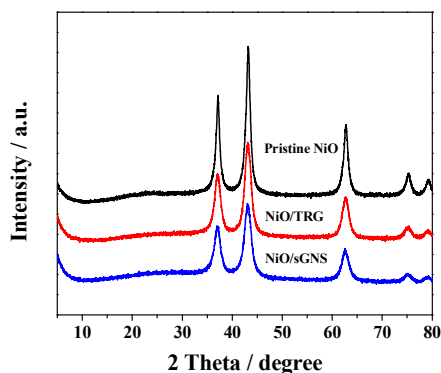


Fig. 1 XRD patterns of pristine NiO, NiO/TRG composites and NiO/sGNS composites.

The microstructures and morphologies of pristine NiO, NiO/TRG composites and NiO/sGNS composites are observed using SEM and TEM in Fig. 2. The wavy nanosheets of sGNS are ultrathin as few layers are overlapped with each other in Fig. 2(a), demonstrating the similar hierarchical structure of sGNS to conventional graphene obtained by the chemical method.³¹⁻³⁴ As seen in Fig. 2(b), the size of pristine NiO nanoparticles with irregular sphere is in the range of around 8 to 11 nm, due to the lack of external pressure stress. In the presence of TRG, Fig. 2(c) show that NiO nanoparticles are reduced in size to around 5 nm, and dispersed on the surface of TRG as the formation of slight aggregation. The changes of NiO nanoparticles resulting from the addition of sGNS are revealed in Fig. 2(d). Surprisingly, NiO nanoparticles in the SEM image of NiO/sGNS composites exhibit the more uniform distribution on the surface of sGNS, as well as the maximum size of 3 nm in the TEM image. The morphology transformation of NiO is closely related to the chemical structure of graphene-based materials. During the assembly process of NiO/TRG composites, metal ions are imbibed into the empty space between carbon nanosheets of TRG by capillary forces for the poor polarity of absolute alcohol. Hence, the agglomeration of NiO with the size shrink is retarded depending on toughness properties of carbon nanosheets. Moreover, the chemical adsorption of nickel cations on the surface of carbon nanosheets based on bonding interaction also plays a vitally important role in curtailing further the dimension expansion of NiO. Sulfonic groups anchored on the surface of sGNS are capable of trapping nickel cations by the formation of coordinate bonding, and hence provide the extra stress to limit the growth of NiO nanoparticles and ensure the uniform dispersion on the surface of carbon nanosheets.

The N_2 sorption isotherms in Fig. 3 illustrate the considerable influence of sGNS on the porous structure of graphene-based composites. As seen above, all the samples exhibit a type IV isotherm corresponding to the presence of a

mesoporous structure. The relative pressure range of NiO/sGNS composites for a hysteresis region is broadened in comparison with those of other samples, implying that the chemical adsorption of nickel cations on sGNS in the fabrication process serves to the diversification of the pore size in the composites. Among all the samples, NiO/sGNS composites exhibit the highest specific surface for the enhanced specific surface of sGNS compared with TRG.³⁵ The pore size distribution curve of NiO/sGNS composites reveals a series of peaks in the pore diameter range of 2 to 10 nm as the peaks of pristine NiO at around 5 nm and NiO/TRG composites at around 3 nm, demonstrating that the addition of sGNS leads to the hierarchical porous structure of the composites and hence benefits the accessibility of electrolytes. Moreover, the pore volumes of pristine NiO, NiO/TRG composites and NiO/sGNS composites are 0.32, 0.88 and 0.78 $\text{cm}^3 \text{g}^{-1}$ respectively, corresponding to the pore lengths of 4.5, 4.1 and 2.9 nm respectively. This result suggests that the unique structure of NiO/sGNS composites caused by the enhanced coordination bonding between nickel cations and sGNS in the absent of water can obviously short the diffusion path of hydroxide ions in the composites during Faradic reaction processes.

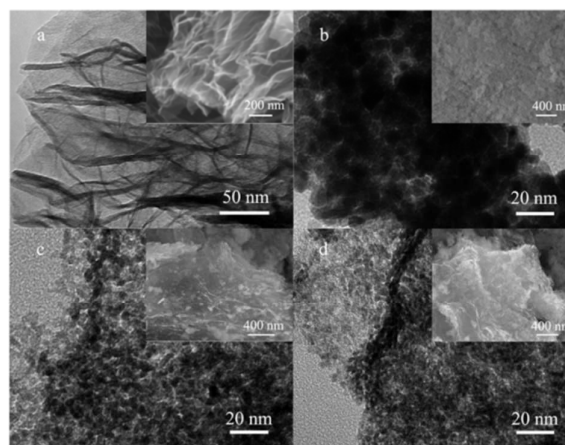


Fig. 2 SEM and TEM images of (a) sGNS, (b) pristine NiO, (c) NiO/TRG composites and (d) NiO/sGNS composites.

To further clarify the difference of all the samples in the surface chemical environment, the X-ray photoelectron spectroscopy experiment is carried out. Fig. 4(a, b, c) shows that the Ni $2p_{3/2}$ peaks observed in pristine NiO and its composites appear at around 853.7 and 855.5 eV. The two components are ascribed to Ni-O bonds and Ni-OH bonds respectively, which is consistent with previous reports.^{36, 37} However, all the samples have distinct difference in the relative intensity between these two peaks, due to the potential effect of two-dimension carbon materials on the chemical structure of metal oxide. Fig. 4(d) shows that the ration of peak 1 to peak 2 is drastically increased in both the composites compared with pristine NiO, which suggests a higher surface hydroxylation of NiO in the composites contributing to improve the compatibility between electrodes

and electrolytes. Moreover, the contribution of NiO/sGNS composites at 856.1 eV is most prevalent, confirming that sulfonic groups anchored on the surface of sGNS are in favor of the surface activated process of NiO. Fig. 5 shows the S 2p region for sGNS and NiO/sGNS composites. The peaks at around 169.0, 166.8 and 164.1 eV are assigned to sulfonic acid, sulfoxide and thioether groups, respectively.³⁸ The appearance of sulfonic acid groups in NiO/sGNS composites confirms that the chemical structure of sGNS possesses the moderate thermostability, when they are partially oxidized to sulfoxide groups during the thermal treatment process.

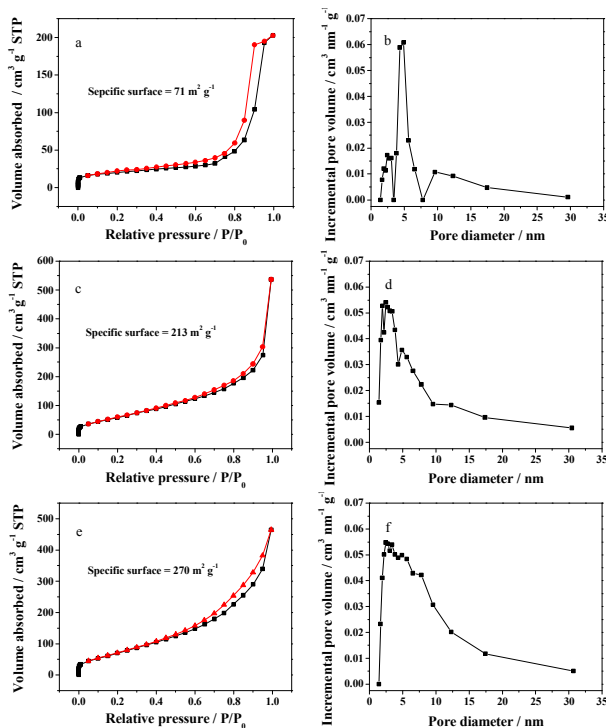
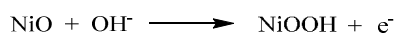


Fig. 3 N₂ adsorption-desorption isotherms of (a) pristine NiO, (c) NiO/TRG composites and (e) NiO/sGNS composites, as well as the pore size distribution curves of (b) pristine NiO, (d) NiO/TRG composites and (f) NiO/sGNS composites.

Considering the effect of the unique structural feature on electrochemical performance of NiO/sGNS composites for supercapacitors, CV curves of three samples are collected at different scan rates of 10, 20 and 30 mV s⁻¹ to investigate their electrochemical behaviors. As indicated in Fig. 6, a pair of current peaks can be clearly identified during the cathodic and anodic sweep processes, which corresponds to the reversible reaction of Ni²⁺ to Ni³⁺ that occurs at the surface of NiO contained in the electrode and can be expressed as follows:^{9, 11}



In addition, the peak intensity increases with an increase in the scan rate, which is consistent with a type pseudocapacitive characteristic. It should be noted that NiO/TRG composites exhibit the higher cathodic current density at the peak potential of around 0.35 V with respect to Hg/HgO electrode

compared with pristine NiO, due to insulating NiO has the rich electrical wiring of conductive carbon nanosheets and achieves the greatly enhanced electrical contact in the composites. However, the electrochemical behavior of NiO/sGNS composites differs from that of NiO/TRG composites. Despite NiO/sGNS composites exhibit the similar redox peak current densities to NiO/TRG composites, the excess response currents of NiO/sGNS composites originating from electrical double-layer capacitive processes contribute to amplify the integral area of the capacitive loop. The improvement of capacitive properties for NiO/sGNS composites is attributed to that the porous structure of NiO/sGNS composites facilitates the adsorption of ions on the surface of electrodes and the diffusion of ions in hierarchical transport channels of electrodes.

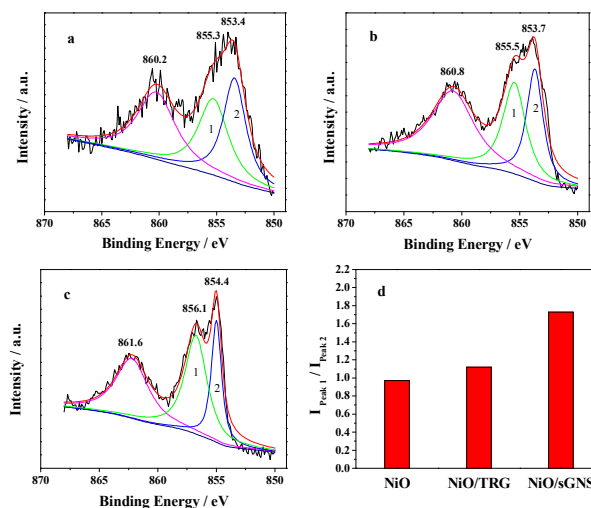


Fig. 4 Ni 2p XPS spectra of (a) pristine NiO, (b) NiO/TRG composites and (c) NiO/sGNS composites, as well as (d) the ratio of peak 1 to peak 2 for all the samples.

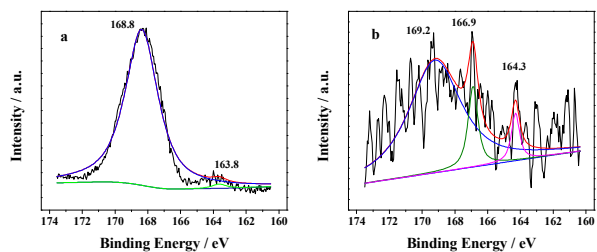


Fig. 5 S 2p XPS spectra of (a) sGNS and (b) NiO/sGNS composites.

The galvanostatic charge-discharge tests of all the electrodes are performed within a stable potential window of 0-0.5 V at different current densities ranging between 1.0 and 5.0 A g⁻¹ in Fig. 7, to demonstrate improved electrochemical performance of composite electrodes. The potential-time plots show mainly characteristic curves of a pseudocapacitor, rather than an electrical double-layer capacitor. The values of C_s are calculated from charging-discharging curves using the equation as follow:

$$C_s = \frac{I \times \Delta t}{m \times \Delta V}$$

where C_s , I , t , V and m are the specific capacitance ($F g^{-1}$), the constant current (A), the discharge time (s), the total potential difference (V) and the mass of the active material in the electrode (g) respectively.

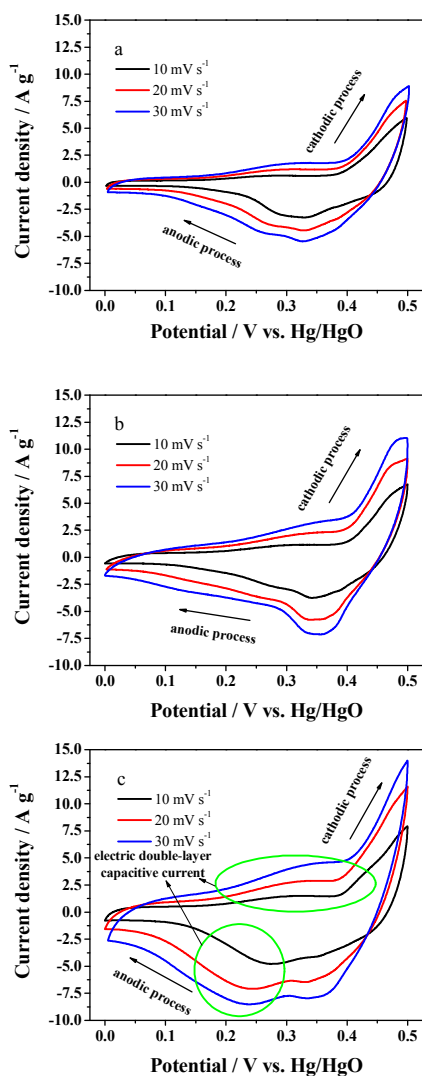


Fig. 6 CV curves of (a) pristine NiO, (b) NiO/TRG composites and (c) NiO/sGNS composites at different scan rates of 10, 20 and 30 $mV s^{-1}$.

The maximum values of C_s are found to be 238, 382 and 530 $F g^{-1}$ for pristine NiO, NiO/TRG composites and NiO/sGNS composites at a current density of 1.0 $A g^{-1}$. Regarding to the significance of a fast charging-discharging process on pseudocapacitive materials, specific capacitances are observed with the increase of current densities. Specific capacitances of pristine NiO, NiO/TRG composites and NiO/sGNS composites are maintained at 152, 244 and 340 $F g^{-1}$ at a current density of 5.0 $A g^{-1}$. As well known, ions in the electrolytes can penetrate into the inner-structure of electrode materials at low current

densities and hence access to almost all available materials of the electrode. However, an effective utilization of the material is only limited to the outer-surface of electrodes in a fast charging-discharging process. In this regard, the improved capacitance of the composites is ascribed to the fact that the porous structure caused by the addition of sGNS provides the adequate transport channels for the diffusion of ions through the rough surface of the electrode during Faradic reaction processes at different current densities. The cycle stability of NiO/sGNS composites is analysed at a current density of 5.0 $A g^{-1}$ in Fig. 8(a). The cyclability test indicates the good stability of NiO/sGNS composites after 1000 cycles and the specific capacitance is stabilized at 327 $F g^{-1}$ resulting in only 3.9 % of the capacitance loss. This result demonstrates that the presence of sGNS is beneficial to maintain the structural integrity of the composites.

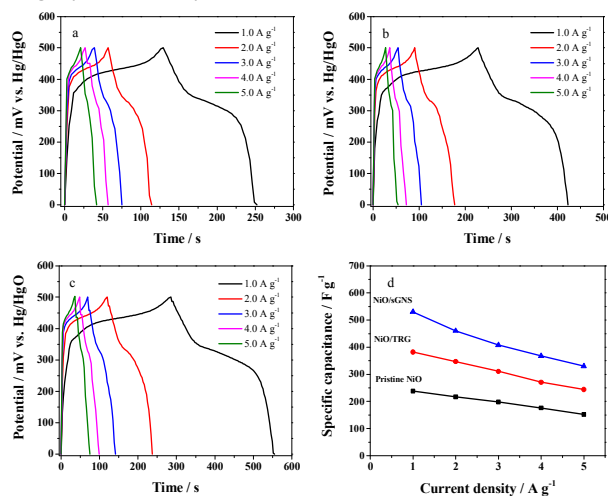


Fig. 7 Galvanostatic charge-discharge curves of (a) pristine NiO, (b) NiO/TRG composites, (c) NiO/sGNS composites at various current densities of 1.0, 2.0, 3.0, 4.0 and 5.0 $A g^{-1}$, (d) the plots of specific capacitances for all the samples following the increase of current densities.

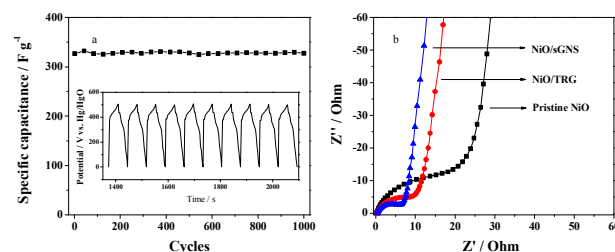


Fig. 8 (a) Cycle life of NiO/sGNS composites at a current density of 5.0 $A g^{-1}$, (b) Nyquist plots of pristine NiO, NiO/TRG composites and NiO/sGNS composites.

The electrical conductivity and ion transfer of supercapacitive electrodes have been further investigated by EIS. Fig. 8(b) shows that Nyquist plots of all the samples consist of two distinct regions following the order of decreasing frequencies. The semicircle in the high frequency region is related to charge transfer resistance (R_{ct}) caused by Faradic reaction. The diameters of semicircles for pristine NiO, NiO/TRG composites

and NiO/sGNS composites are 24.8, 9.9 and 7.1 Ohm, indicating that the electrical interconnection led by the combination of NiO and sGNS in the composites contributes to the diffusion of electric charges at the surface of the electrode during Faradic reaction processes. The inclined line in the low frequency region corresponds to diffusive resistance of the electrolyte in the electrode (Warburg impedance, W). The phase angles of the impedance plots for pristine NiO, NiO/TRG composites and NiO/sGNS composites are found to be sequentially increased, due to that the porous structure of NiO/sGNS composites provides abundant variations in ion diffusion paths and benefits the movement of ions within the pores.

4. Conclusion

In the summary, porous NiO/sGNS composites are successfully fabricated utilizing ammonium carbamate as a precipitating agent. In the absence of water, sulfonated graphene reveal the potential control ability on the specific surface of the composites and the surface chemical environment. The addition of sGNS not only enhances the specific surface of the composites and broadens the pore size distribution, but also strengthens the surface hydroxylation of NiO in the composites. The peculiar structure of NiO/sGNS is capable to provide sufficient channels for the transfer of electrons in the electrode and favor the movement of ions to the inner-structure of composite electrodes. As expected, NiO/sGNS electrode among all the samples exhibits the highest specific capacitance of 530 F g^{-1} and the excellent cycling stability with 3.9 % of the capacitance loss after 1000 cycles.

Acknowledgements

The above work was supported by China Postdoctoral Science Foundation (No. 2014M551047), National Natural Science Foundation of China (No.21403189), Hebei province natural science foundation of China (No. B2012203005, E2015203089), Key Technology Research and Development Program of Qinhuangdao (No. 201401A004).

Notes and references

a Hebei Key Laboratory of Applied Chemistry, College of Environmental and Chemical Engineering, Yanshan University, Qinhuangdao, 066004, China. Fax: 86 335 8061569; Tel: 86 335 8061569; E-mail: chinalinkwuang@126.com.

b The State Key Laboratory of Electroanalytic Chemistry, Changchun Institute of Applied Chemistry, Chinese Academy of Sciences, Changchun, 130022, China. Tel: 86 431 85262632; Email: wucunqi@ciac.ac.cn.

- 1 H.L. Wang, H.S. Casalongue, Y.Y. Liang, H.J. Dai, *J. Am. Chem. Soc.*, 2010, 132, 7472-7477.
- 2 S. Teng, G. Siegel, M.C. Prestgard, W. Wang, A. Tiwari, *Electrochim. Acta*, 2015, 161, 343-350.
- 3 L. O'Neill, C. Johnston, P.S. Grant, *J. Power Sources*, 2015, 274, 907-915.
- 4 M. Jana, S. Saha, P. Khanra, P. Samanta, H. Koo, N.C. Murmu, T. Kuila, *J. Mater. Chem. A*, 2015, 3, 7323-7331.

- 5 P. Hao, Z.H. Zhao, J. Tian, H.D. Li, Y.H. Sang, G.W. Yu, H.Q. Cai, H. Liu, C.P. Wong, A. Umar, *Nanoscale*, 2014, 6, 12120-12129.
- 6 X.H. Liu, L. Zhou, Y.Q. Zhao, L. Bian, X.T. Feng, Q.S. Pu, *ACS Appl. Mater. Interfaces*, 2013, 5, 10280-10287.
- 7 I. Nam, G.P. Kim, S. Park, J.W. Han, J. Yi, *Energy Environ. Sci.*, 2014, 7, 1095-1102.
- 8 Y. Wang, Z.Q. Shi, Y. Huang, Y.F. Ma, C.Y. Wang, M.M. Chen, Y.S. Chen, *J. Phys. Chem. C*, 2009, 113, 13103-13107.
- 9 K.K. Purushothaman, I.M. Babu, B. Sethuraman, G. Muralidharan, *ACS Appl. Mater. Interfaces*, 2013, 5, 10767-10773.
- 10 G.A. Babu, G. Ravi, T. Mahalingam, M. Kumaresavanji, Y. Hayakawa, *Dalton Trans.*, 2015, 44, 4485-4497.
- 11 S. Vijayakumar, S. Nagamuthu, G. Muralidharan, *ACS Appl. Mater. Interfaces*, 2013, 5, 2188-2196.
- 12 J.T. Li, W. Zhao, F.Q. Huang, A. Manivannan, N.Q. Wu, *Nanoscale*, 2011, 3, 5103-5109.
- 13 S. Vijayakumar, S. Nagamuthu, G. Muralidharan, *ACS. Sustain. Chem. Eng.*, 2013, 1, 1110-1118.
- 14 N. Chopra, W.W. Shi, A. Bansal, *Carbon*, 2011, 49, 3645-3662.
- 15 Y. Cheng, P.K. Shen, S.P. Jiang, *Int. J. Hydrogen Energy*, 2014, 39, 20662-20670.
- 16 X.F. Lu, J. Lin, Z.X. Huang, G.R. Li, *Electrochim. Acta*, 2015, 161, 236-244.
- 17 F. Chen, W.J. Zhou, H.F. Yao, P. Fan, J.T. Yang, Z.D. Fei, M.Q. Zhong, *Green Chem.*, 2013, 15, 3057-3063.
- 18 X.Y. Wang, X.Y. Wang, L.H. Yi, L. Liu, Y.Z. Dai, H. Wu, *J. Power Sources*, 2013, 224, 317-323.
- 19 C.G. Liu, Z.N. Yu, D. Neff, A. Zhamu, B.Z. Jang, *Nano Lett.*, 2010, 10, 4863-4868.
- 20 J.L. Huang, J.Y. Wang, C.W. Wang, H.N. Zhang, C.X. Lu, J.Z. Wang, *Chem. Mater.*, 2015, 27, 2107-2113.
- 21 P.Q. Cao, L.C. Wang, Y.J. Xu, Y.B. Fu, X.H. Ma, *Electrochim. Acta*, 2015, 157, 359-368.
- 22 Y.M. Chen, Z.D. Huang, H.Y. Zhang, Y.T. Chen, Z.D. Cheng, Y.B. Zhong, Y.P. Ye, X.L. Lei, *Int. J. Hydrogen Energy*, 2014, 39, 16171-16178.
- 23 C. Bora, J. Sharma, S. Dolui, *J. Phys. Chem. C*, 2014, 18, 29688-29694.
- 24 J.L. Lu, W.S. Liu, H. Ling, J.H. Kong, G.Q. Ding, D. Zhou, X.H. Lu, *RSC Advances*, 2012, 2, 10537-10543.
- 25 Q. Wu, Y.Q. Sun, H. Bai, G.Q. Shi, *Phys. Chem. Chem. Phys.*, 2011, 13, 11193-11198.
- 26 B. Ma, X. Zhou, H. Bao, X.W. Li, G.C. Wang, *J. Power Sources*, 2012, 215, 36-42.
- 27 L. Wang, H. Tian, D.L. Wang, X.J. Qin, G.J. Shao, *Electrochim. Acta*, 2015, 151, 407-414.
- 28 W.S. Hummers, R.E. Offeman, *J. Am. Chem. Soc.*, 1958, 80, 1339-1339.
- 29 Q.L. Du, M.B. Zheng, L.F. Zhang, Y.W. Wang, J.H. Chen, L.P. Xue, W.J. Dai, G.B. Ji, J.M. Cao, *Electrochim. Acta*, 2010, 55, 3897-3903.
- 30 Y.C. Si, E.T. Samulski, *Nano Lett.*, 2008, 8, 1679-1682.
- 31 M.D. Stoller, S.J. Park, Y.W. Zhu, J.H. An, R.S. Ruoff, *Nano Lett.*, 2008, 8, 3498-3502.
- 32 D.W. Wang, F. Li, Z.S. Wu, W.C. Ren, H.M. Cheng, *Electrochem. Commun.*, 2009, 11, 1729-1732.
- 33 J. Yan, Z.J. Fan, T. Wei, W.Z. Qian, M.L. Zhang, F. Wei, *Carbon*, 2010, 48, 3825-3833.
- 34 M.S. Park, J.S. Yu, K.J. Kim, G.J. Jeong, J.H. Kim, Y.N. Jo, U. Hwang, S. Kang, T. Woob, Y.J. Kim, *Phys. Chem. Chem. Phys.*, 2012, 14, 6796-6804.
- 35 H.B. Li, Y. Wang, Y.M. Shi, J. Li, L.J. He, H.Y. Yang, *RSC Adv.*, 2013, 3, 14954-14959.

Journal Name

ARTICLE

- 36 K.B. Wang, Z.Y. Zhang, X.B. Shi, H.J. Wang, Y.N. Lu, X.Y. Ma, *RSC Adv.*, 2015, 5, 1943-1948.
- 37 A.K. Singh, D. Sarkar, G.G. Khan, K. Mandal, *ACS Appl. Mater. Interfaces*, 2014, 6, 4684-4692.
- 38 A.J. Crisci, M.H. Tucker, M.Y. Lee, S.G. Jang, J.A. Dumesic, S.L. Scott, *ACS Catal.*, 2011, 1, 719-728.